JCIM JOURNAL OF CHEMICAL INFORMATION AND MODELING

pubs.acs.org/jcim Article

Exploring Chloride Selectivity and Halogenase Regioselectivity of the SalL Enzyme through Quantum Mechanical/Molecular Mechanical Modeling

Paulo R. M. Pereira, Jéssica de O. Araújo, José Rogério A. Silva, Cláudio N. Alves, Jerônimo Lameira, and Anderson H. Lima*

Cite This: J. Chem. Inf. Model. 2020, 60, 738−746 Read Online

ACCESS | Metrics & More | Article Recommendations | Supporting Information

ABSTRACT: The catalytic mechanism of SalL chlorinase has been investigated by combining quantum mechanical/molecular mechanical (QM/MM) techniques and umbrella sampling simulations to compute free energy profiles. Our results shed light on the interesting fact that the substitution of chloride with fluorine in SalL chlorinase leads to a loss of halogenase activity. The potential of mean force based on DFTB3/MM analysis shows that fluorination corresponds to a barrier 13.5 kcal·mol^{-1} higher than chlorination. Additionally, our results present a molecular description of SalL acting as a chlorinase instead of a methyl-halide transferase.

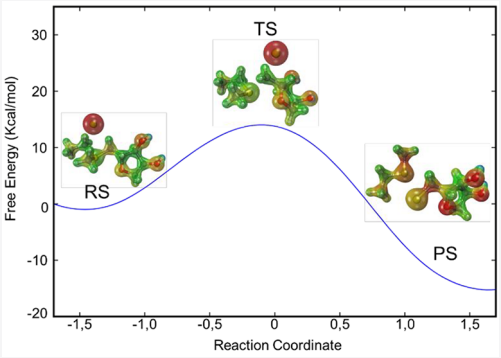

INTRODUCTION

Methyltransferases and halogenases play important roles in normal physiology and human diseases.[1,2] This class of enzymes uses a bimolecular nucleophilic substitution (S_N2) methyl transfer mechanism, where *S*-adenosyl-L-methionine (AdoMet or SAM) donates a methyl to a nitrogen, oxygen, or halogen atom.[3] Particularly, some studies have investigated the potential of halogenase enzymes, responsible for the biosynthesis of halogenated natural products, as biocatalysts.[4,5] There are a number of fundamentally different classes of halogenases, which are categorized on the basis of the mechanism by which they generate and utilize activated halide.[5,6] For example, the enzyme Chlorinase SalL halogenates *S*-adenosyl-L-methionine (SAM) with chloride to generate 5′-chloro-5′-deoxyadenosine and L-methionine[7] (Scheme 1a). On the other hand, SAM-dependent halide methyltransferases can utilize SAM to produce halomethanes, CH_3X (X = Cl, Br, I)[8] (Scheme 1b). The SN_2 reaction represented in Scheme 1a is analogous to that observed in *Streptomyces cattleya* fluorinase[9] and is associated with the biosynthesis of the potent proteasome inhibitor salinosporamide A, a chlorinated anticancer candidate.[10]

It is well-known that the chlorinase SalL accepts Cl^-, Br^-, and I^-, but not F^- as nucleophilic groups.[6,7] It determines the nature of reaction products, where the chlorinase SalL produces, mainly, 5′-chloro-5′-deoxyadenosine and not chloromethane, as presented in Scheme 1b.

Recently, the origin of the catalytic effect of methyltransferases has been explored successfully by using QM/MM and free energy surface approaches.[11−13] In this study, the QM/MM method at the DFTB3/AMBER level has been used to provide a detailed molecular insight into the selectivity of the SalL chlorinase enzyme in the presence of two particular ions (Cl^- and F^-). This provides access to a comparison of the free energy barrier for the possible mechanism pathways which could be promoted by the catalytic site of the SalL chlorinase enzyme, where selectivity and regioselectivity are deeply explored. We have shown that SalL activity and regioselectivity are well reproduced by our theoretical results, providing a detailed molecular rationalization. Considering the fact that halogenated organic compounds have been attractive for pharmaceuticals and agrochemicals by different benefits, we have discussed the relevance of our results for understanding the mechanisms of SalL halogenation.

COMPUTATIONAL METHODS

Modeling the Initial Structures. The complex SalL with SAM and Cl^- was modeled from a SalL−Y70T X-ray crystallographic structure that was obtained from the Protein Data Bank[14] (PDB code 2Q6O).[7] The native structure has been obtained by replacing the Tyr70 by a Thr residue. The complex

Special Issue: Molecular Simulation in Latin America: Coming of Age

Received: November 21, 2019
Published: January 13, 2020

Scheme 1. (a) Representation of the Halogenation of SAM to Generate L-Methionine (L-MET) and 5-Chloro-5-deoxyadenosine (5′-ClDA) and (b) Reaction between Halide Ion (X^- = Cl^-, Br^-, and I^-) and SAM to Generate Halomethane

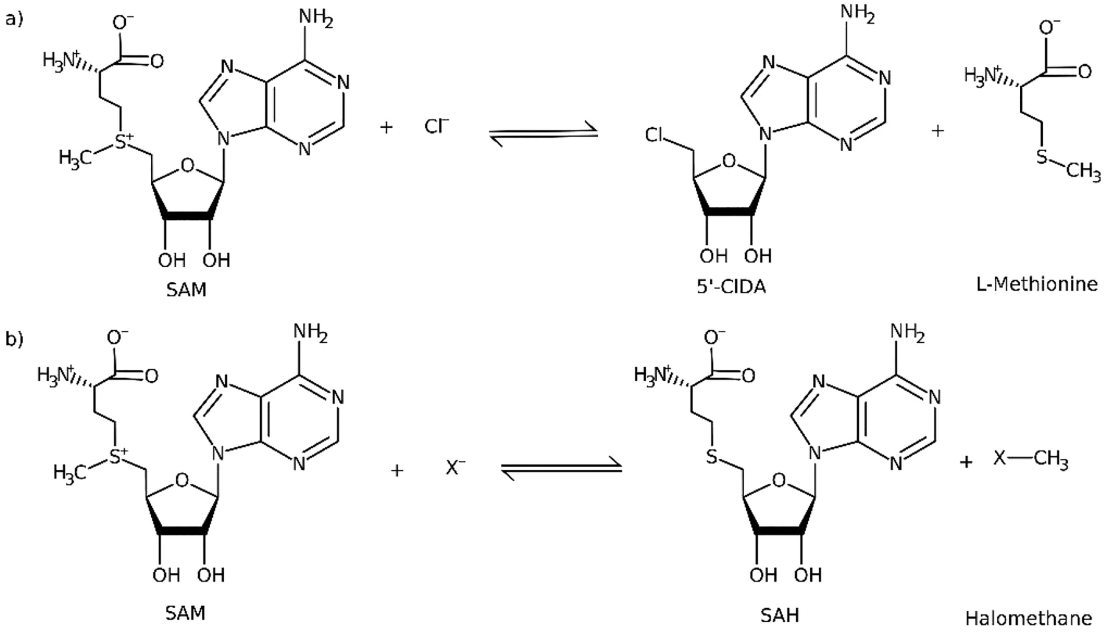

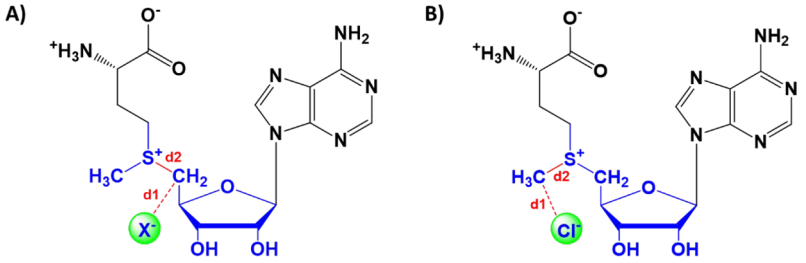

Figure 1. Distances used to scan the 1D reaction coordinate. (A) d1 refers to the distance between the nucleophile Cl^- or F^- and the C5′ atom of SAM. d2 is the distance between the S and C5′ atoms of SAM. (B) d1 refers to the distance between the nucleophile Cl^- and CE atom of SAM. d2 is the distance between the S and CE atoms of SAM. Atoms colored blue represents the QM region of the QM/MM partitioning. Hydrogen atoms were used to link QM and MM regions of the system.

SalL with SAM and F^- was modeled by substituting the Cl^- for F^- in the active site. Hydrogen atoms of enzyme−substrate complexes were added by the tLeap module of Amber16. The protonation states of acidic and basic residues were determined under pH 7.0 condition and analyzed by H++ server.[15] All-atom force field (AMBER ff14SB)[16] and general amber force field (GAFF)[17] were used to describe SalL and SAM, respectively. The SAM charges were calculated on the Gaussian 09 software suite[18] using the Hartree−Fock method with 6-31G* basis.[19] The systems were solvated in a truncated octahedral water-box with the explicit solvation model TIP3P.[20] We used a distance of 12.0 Å between the cell wall and the solvated atoms of the system. Counterions were also added to neutralize the system.

QM/MM MD and Free Energy Simulations. Semi-empirical QM/MM calculations were performed using the DFTB3 Hamiltonian[21] for atoms in the quantum region. For all QM/MM calculations, the QM region consisted of the ligand (SAM) and the ions Cl^- or F^-. The hydrogen "link atom" was used to model the bond across the QM/MM boundary (See Figure 1). The total charge of the QM region was 0. The initial structures of the complexes were minimized first by 10 000 cycles of steepest descent and conjugate gradient[22] algorithms with restraints on the coordinates of the QM atoms. Then, the whole system was minimized with the progressive relaxation of restraints. We used 20 ps to raise the temperature gradually from 10 to 300 K. Afterward, 50 ps of unrestrained QM/MM MD simulations were carried out for reactant state (RS) complexes. It was performed using periodic boundary conditions with a cutoff distance of 12.0 Å and a time step of 1.0 fs.

Further umbrella-sampling MD simulations were then performed (at the DFTB3/ff14SB level) in order to calculate the activation barrier for the nucleophilic attack of Cl^- on C5′ atom bonded to the sulfur atom of SAM (see a detailed scheme of reaction coordinates for this study in Figure 1). Coordinates and velocities obtained after 5 ps of simulation (equilibration runs) for the first reaction coordinate value were used to start the simulation for the next reaction coordinate value. The simulation was divided into 35 windows with each window simulated for 60 ps (production runs). The reaction coordinate ξ = d (S−C5′) − (Cl−C5′), was constrained using a force constant of 500 kcal/mol Å^2 and scanned from −1.70 to 1.70 Å in steps of 0.10 Å. The same procedure was used to investigate the nucleophilic attack of F^- on C5′. Finally, the nucleophilic attack of Cl^- on CE atom of SAM to produce chloromethane and *S*-adenosyl-L-homocysteine (SAH) was investigated with the reaction coordinate ξ = d (S−CE) − (Cl−CE).

https://dx.doi.org/10.1021/acs.jcim.9b01079
J. Chem. Inf. Model. 2020, 60, 738−746

Free energy profiles were obtained from these simulations using the weighted-histogram analysis method[23] with a convergence tolerance of 0.000 01 and a temperature of 300 K. The boundaries of the histogram were −1.70 to 1.70 and the numbers of bins were set to 1000. The transition state was identified as the highest energy point along with the free energy profile.

In order to validate the semiempirical level of theory implemented in QM/MM calculations, single-point calculations at M06-2X-D3/MM level were carried out using 400 snapshots from reactant and transition states obtained from free energy profiles at DFTB3/MM level, which has been applied on previous enzymatic studies.[24−27] The correction added to the free energy profiles was computed by using a straightforward one-step free energy perturbation:

$$\Delta G_{\mathrm{M062X-DFTB3}} = -k_{\mathrm{B}}T\ln\langle e^{-\beta(E_{\mathrm{M062X/MM}}-E_{\mathrm{DFTB3/MM}})}\rangle_{\mathrm{DFTB3/MM}} \quad (1)$$

Residual Decomposition Analysis. The energy decomposition method to analyze how the enzymatic environment stabilizes or destabilizes the transition state (TS) in the catalyzed reaction of SalL with SAM in the presence of Cl^- or F^- ions. This approach has been successfully applied to enzyme systems.[28,29] In this procedure, the energetic contribution of an individual residue on the total energy of a particular structure is computed by using the difference of energies when this particular residue is present (i state) and when it is replaced by Gly residue ($i-1$ state),[30,31] according to eq 1:

$$\Delta E_i = [E_i - E_{i-1}]_{\mathrm{QM}} + [E_i - E_{i-1}]_{\mathrm{QM/MM}} \quad (2)$$

where each term in brackets represents the difference energy of the subsystem treated by the QM level in the presence of the classical environment and the interaction energy between the QM and MM part. Therefore, the stabilization effects in going from R to TS, for each residue, were calculated by eq 3:

$$\Delta\Delta E_i = \Delta E_i^{\mathrm{TS}} - \Delta E_i^{\mathrm{R}} \quad (3)$$

Here, the QM subsystem was described previously on the umbrella sampling MD simulations and the average values for the interaction energy and stabilization effects were computed from 400 snapshots from MD simulations taken from the QM/MM umbrella sampling with reaction coordinates corresponding to the R and TS states.

RESULTS AND DISCUSSION

QM/MM Free Energy Profiles for Chloride Selectivity. The SalL enzyme, a homologue that shares 35% sequence identity with 5′-fluoro-5′-deoxyadenosine synthase, has been shown to catalyze chlorination under native conditions but does not catalyze fluorination.[7,32] Kinetic properties have been determined experimentally for SalL chlorinase from *Salinispora tropica* (k_{cat} 0.9 ± 0.1 min^{-1} for Cl^- and activity not detected for F^-).[7] Thus, that kinetic constant means a barrier of $\Delta G^{\ddagger} \sim 20.06$ kcal/mol using Transition State Theory.[33] The free energy profiles for reactions in the enzyme are presented in Figure 2.

The free energy of activation for a reaction involving SalL and Cl^- corresponds to 17.57 kcal/mol, while the barrier for a reaction involving SalL and F^- is 30.90 kcal/mol. The calculated activation free energies for reactions in protein are in reasonable agreement with the corresponding experimental values described above. In order to evaluate the convergence of the calculated PMF, we have computed $\Delta G^{\ddagger}$ for each reaction using different sampling times (20, 40, and 60 ps) for each US window. The results show that sampling obtained from 40 ps of MD simulations is similar to sampling for 60 ps for all systems studied (see Table S1).

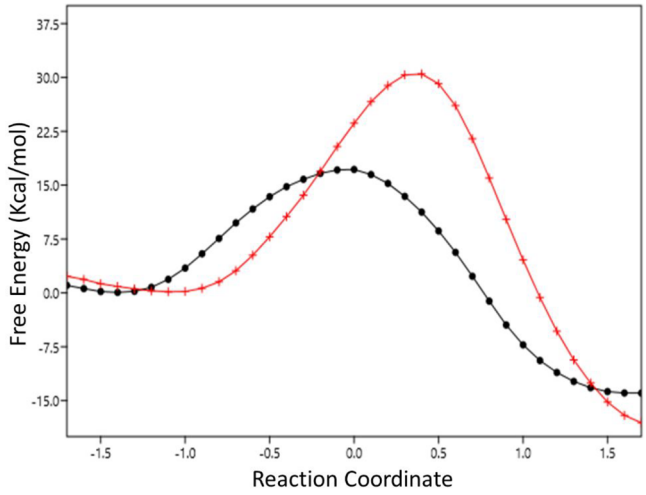

Figure 2. Free energy profiles calculated at DFTB3/MM level for the reaction of SAM with Cl^- (black line) or F^- (red line) catalyzed by the SalL enzyme.

The reaction catalyzed by the native enzyme reveals that the thermodynamic profile is exergonic ($\Delta G = -14.10$ kcal/mol), as shown in Figure 2. Considering the nucleophilic attack of F^- to C5′, the difference between the activation free energies ($\Delta\Delta G^{\ddagger}$), is about ∼13.5 kcal/mol, showing that it is a kinetically unfavorable reaction and agrees with the experimental data that shows no reactivity observed.[7] The free energy barriers obtained by the corrected PMFs using M06-2X-D3/6-31G* as high QM level are 14.51 and 29.32 kcal/mol for the SaIL−Cl and SaIL−F systems, respectively, showing that DFTB3 is in good agreement to high theory level as DFT. It reproduces the same trend in the difference in activation free energy of the reactions with chloride and fluoride ions ($\Delta\Delta G^{\ddagger} \sim 14.8$ kcal/mol).

According to results obtained from umbrella sampling simulations, structural analysis suggests that Tyr70 and Gly131 residues appear to stabilize the TS by interacting with the nucleophilic group (Cl^- or F^- ion). Even though previous computational study underestimates the true value of SalL chlorination of SAM, they revealed the importance of the interaction between the chloride and backbone amide of Gly131, which are extremely conserved in DUF62 proteins.[34,35] Replacement of Gly131 by serine to engineer a similarity to the fluorinase resulted in instability and arrested chlorination.[36] The Ser158 (in fluorinase) corresponds to Gly131 in SalL. It was proposed to offset the energetic cost of desolvation of fluoride through compensatory hydrogen bonding.[7] Furthermore, our calculations are in agreement with the idea of a bimolecular nucleophilic S_N2 type substitution mechanism, with a Cl^- ion instead of F^-, where the chloride ion adopts a position approximately 180° from the electrophilic C5′ carbon of SAM, consistent also with an S_N2 mechanism as described for the fluorinase.[36,37]

An overview of the computational studies made for halogenases[38] showed fluorinase able to catalyze the reaction with chlorine, but with higher activation energy ($\Delta\Delta G^{\ddagger}_{\mathrm{exp}} = 12$ kJ/mol against $\Delta\Delta G^{\ddagger}_{\mathrm{calc}} = 10$ kJ/mol).[39] In addition, Senn[38]

https://dx.doi.org/10.1021/acs.jcim.9b01079
J. Chem. Inf. Model. 2020, 60, 738−746

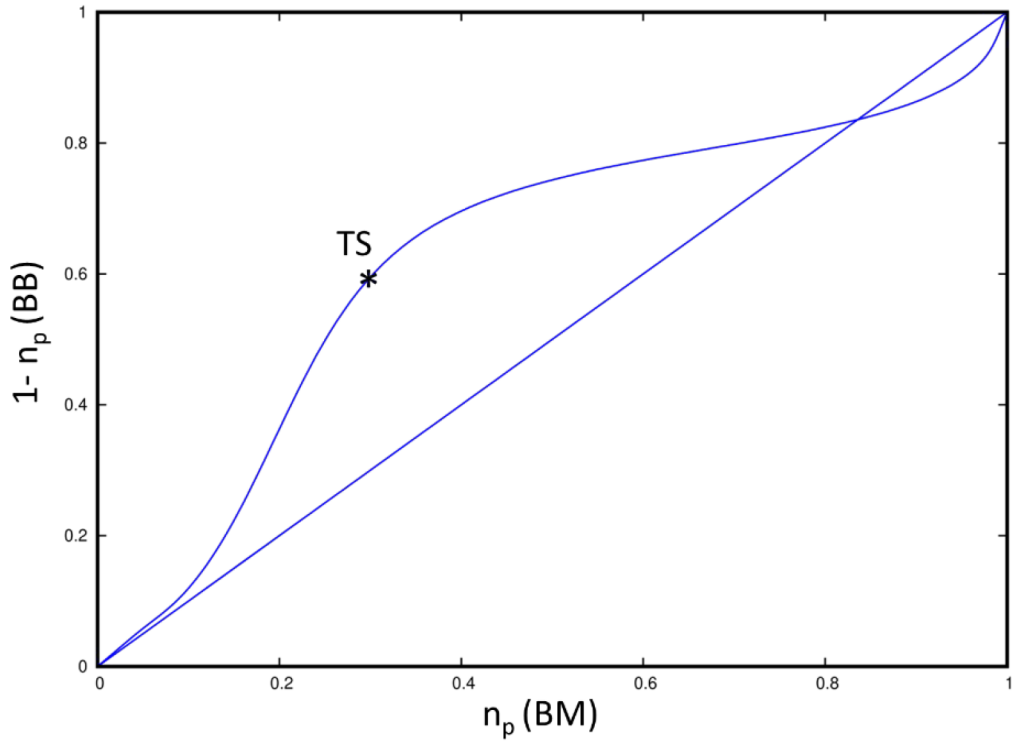

Figure 3. More O'Ferrall−Jencks diagrams of the chlorination of SAM by the SalL enzyme, with coordinates defined using modified Pauling bond orders. The axes are the Pauling bond orders from the S−C5′ bond length $[1 - n_p(\mathrm{BB})]$ and the C5′−Cl^- bond length $n_p(\mathrm{BM})$.

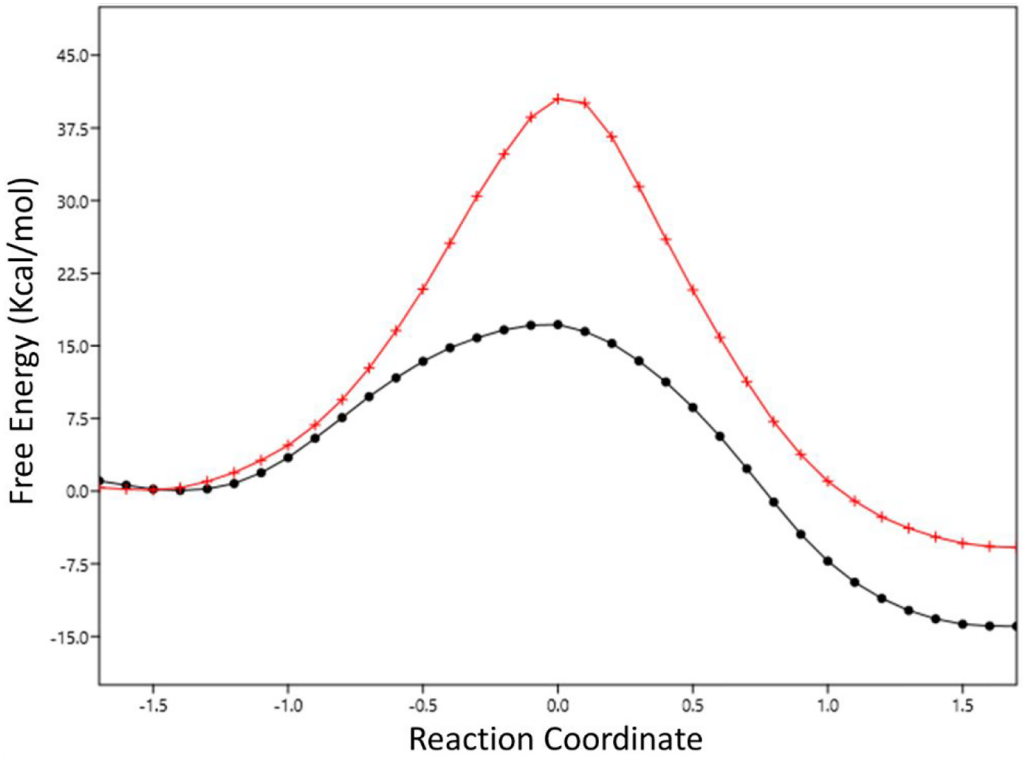

Figure 4. Free energy profiles calculated at DFTB3/MM level for the reaction of SAM with Cl^- attacking C5′ (black line—showing halogenase activity) and attacking CE atom (red line—showing methyl-halide transferase activity).

discusses another study performed by Healy,[40] which shows that the microsolvation of the chloride by one water molecule in the active site reduces its nucleophilicity and may account for the significantly lower activity of the Tyr70Thr mutant compared to the wild-type. Here, our results demonstrate the importance of Tyr70 in giving for support during a nucleophilic attack on the catalytic reaction. Besides, Trp129 residue provides a stabilizing effect for the transition state of the reaction. Energetic

https://dx.doi.org/10.1021/acs.jcim.9b01079
J. Chem. Inf. Model. 2020, 60, 738−746

contributions for stabilizing the reaction will be discussed below. On the other hand, our study presented how SalL chlorinase (a different enzyme from fluorinase) accepts chloride and not fluoride in SAM halogenation. Besides that, we presented a structural and energetic analysis that shows that SalL is unlikely to act as a methyl halide transferase.

In order to understand the real nature of the chlorination of SAM by the SalL enzyme, a "reaction space" plot based on a More O'Ferral–Jenk (MOJ) style diagram[41] was done. It is well-known that a concerted S_N2 mechanism can be described by A_ND_N where the association of the nucleophile and dissociation of the leaving group, each with an unbonded electron pair, are indicated by A_N and D_N, respectively.[42] This approach was used successfully to describe the mechanism of *Trypanosoma cruzi trans*-Sialidase[43] using Pauling bond orders, n_p.[44] Thus, once we have the bond order usually defined as a function of bond length, we define the bond order MOJ diagram with the bond-making axis equal to $n_p(BM)$ and the bond-breaking axis equal to $[1 - n_p(BB)]$.

The partial bond order indices were calculated using eq 4 from the bond lengths of the structures along the minimum free energy path. This equation has been useful in the interpretation of transition state geometries.[43,45]

$$n_p = n_0 \exp[(R_0 - R)/0.6] \quad (4)$$

where R denotes the average distance between the S or Cl^- and the C5′, $n_0 = 1$, $R_0 = 1.8$, and 0.6 is a proportionality constant.

Figure 3 presents the bond orders derived from the original Pauling equation (eq 4). It indicates more bond-breaking than bond-making in the transition state. In other words, we can define the mechanism is a dissociative one, which means that the leaving group departs well before the TS is reached. The bond orders at the TS to the BM and the BB were 0.29 and 0.59, respectively.

QM/MM Free Energy Profiles for SalL Acting As a Methyl-Halide Transferase. In order to evaluate SalL as methyl-halide transferase, we have simulated the nucleophilic attack of Cl^- to CE atom of SAM to obtain chloromethane and SAH as reaction products (Scheme 1b). Due to the SAM sulfonium moiety and the leaving group propensity of the resultant thioether, different enzymes have been identified that catalyze nucleophilic attack at all three carbons (C5′, CE, and C5) of SAM positioned adjacent to this sulfonium sulfur.[36] According to our calculations, by comparing the activation free energy for SalL as a chlorinase and methyl-halide transferase, the highest value of $\Delta G^{\ddagger}$ found was 41.95 kcal/mol for the SalL–halide/thiol methyltransferase (HTMT) system, which is 24.38 kcal/mol higher than the SalL–Cl system (Figure 4). The corrected $\Delta G^{\ddagger}$ value for the SalL–HTMT system computed at the M06-2X-D3/6-31G* level is 42.00 kcal/mol, only 0.05 kcal/mol higher than the DFTB3 result, which demonstrates good agreement between the lower and higher QM levels.

In order to understand the difference between SalL acting as a chlorinase and methyl-halide transferase, the Mulliken charge changes were calculated for ensembles taken from QM/MM umbrella sampling calculations on each stationary point (Table 1).

As the reaction progresses, the atomic charge on C5′ and CE changes from negative to neutral as it becomes attacked by the nucleophile (Cl^- in these cases). As chlorine has a charge of −0.18 au, the C5′–Cl bond has already been formed with the release of energy, as can be seen in Figure 2. On the other hand, a charge of −0.16 au was observed when the CE–Cl bond was already formed. The bond-breaking process shows that in the TS the distance between S and C5′ is 2.41 ± 0.06 Å while the distance between S and CE is 2.54 ± 0.06 Å (Table 2). In addition, it is important to note that the positively charged sulfonium ion, where the S atom has a charge of 0.37 au and 0.38 au for the attack to C5′ and CE, respectively, confers stability to the catalytic site. Thus, a greater charge transfer of the nucleophile in both chlorinase and halogenase action is observed, in which the chloride ion significantly loses its negative charge.

Table 1. Average Mulliken Charges (Calculated at the DFTB3/ff14SB QM/MM Level) in Atomic Units (a.u.) for the Relevant QM Atoms Involved in the Reactions, Averaged from the QM/MM Free-Energy Profile

atom	reactant state	transition state	product state
	SalL–Cl Complex (Attack at the C5′ Atom of SAM)		
Cl	−0.92 ± 0.02	−0.73 ± 0.03	−0.18 ± 0.02
S	0.37 ± 0.03	0.05 ± 0.03	−0.16 ± 0.02
C5′	−0.14 ± 0.02	−0.02 ± 0.02	−0.01 ± 0.01
CE	−0.22 ± 0.02	−0.19 ± 0.01	−0.19 ± 0.01
C5	−0.13 ± 0.02	−0.07 ± 0.01	−0.05 ± 0.01
	SalL–Cl Complex (Attack at the CE Atom of SAM)		
Cl	−0.93 ± 0.02	−0.75 ± 0.05	−0.16 ± 0.03
S	0.38 ± 0.03	0.13 ± 0.04	−0.17 ± 0.02
C5′	−0.14 ± 0.02	−0.10 ± 0.02	−0.09 ± 0.01
CE	−0.21 ± 0.02	−0.08 ± 0.02	−0.08 ± 0.01
C5	−0.12 ± 0.02	−0.08 ± 0.01	−0.06 ± 0.01

Table 2. Distances (Å) that Represent Characteristics of the Reactant Complex, Transition, and Product States[a]

distances	reactant complex	transition state	product state
	SalL–Cl Complex (Attack at the C5′ Atom of SAM)		
d1 (C5′–Cl)	3.35 ± 0.05	2.51 ± 0.05	1.81 ± 0.03
d2 (C5′–S)	1.85 ± 0.04	2.41 ± 0.06	3.42 ± 0.04
	SalL–Cl Complex (Attack at the CE Atom of SAM)		
d1 (CE-Cl)	3.33 ± 0.04	2.57 ± 0.06	1.81 ± 0.03
d2 (CE-S)	1.83 ± 0.04	2.54 ± 0.06	3.41 ± 0.04
	SalL–F Complex (Attack at the C5′ Atom of SAM)		
d1 (C5′-F)	2.95 ± 0.04	2.06 ± 0.09	1.42 ± 0.04
d2 (C5′-S)	1.85 ± 0.04	2.47 ± 0.08	3.13 ± 0.47

[a]Definitions of d1 and d2 are depicted in Figure 1. The values were taken from the MD simulations snapshots related to those configurations.

The nucleophilic attack to CE atom of SAM leads to the formation of S-adenosyl-L-homocysteine (SAH) whose crystal structure has been solved.[46] SAH is devoid of the sulfonium methyl group of SAM, thus, has neutral sulfur, and is an unreactive substrate analog.

Additionally, we have evaluated the influence of the SalL enzyme on the electrostatic potential surfaces of the SAM and Cl^- along with the reaction coordinates, determining the molecular electrostatic potential (MEP) surfaces for it in a protein environment (see Figure 5, and Figure S1 for all MEPs). This strategy has been successfully applied in previous enzymatic systems.[47,48] Here, MEP surfaces were obtained from the M06-2X/6-31G(d) level using representative structures obtained from optimized RS, TS, and PS reaction coordinates. These surfaces correspond to an isodensity value of 0.002 au. The most nucleophilic regions (negative electronic

https://dx.doi.org/10.1021/acs.jcim.9b01079
J. Chem. Inf. Model. 2020, 60, 738–746

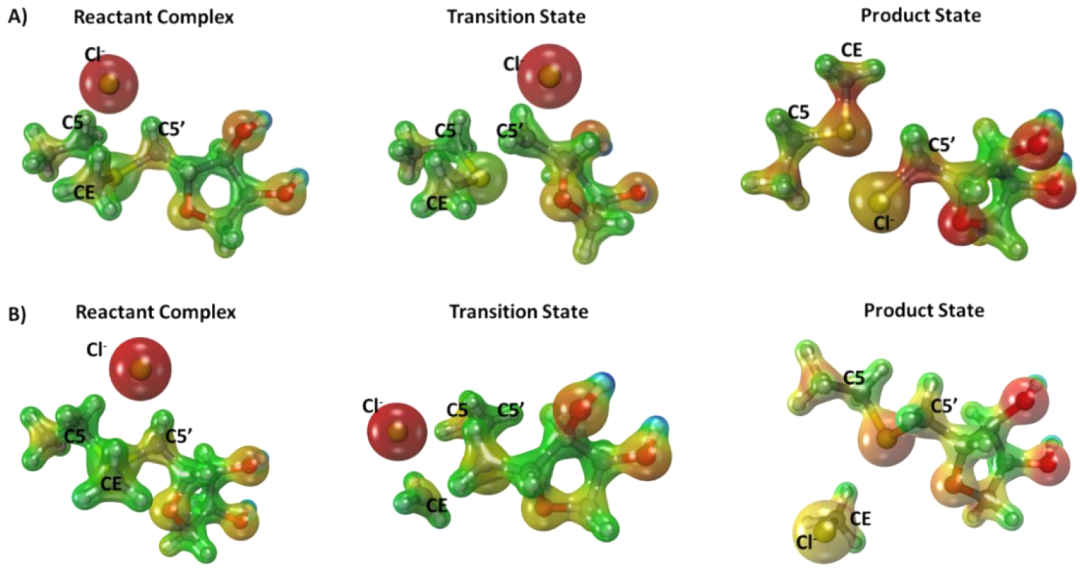

Figure 5. Molecular electrostatic potential (MEP) surfaces derived from M06-2X/6-31G* calculations for (A) chlorination of SAM by the SalL enzyme—attack at the C5′ atom (halogenase action). (B) Chlorination of SAM by the SalL enzyme—attack at the CE atom (methyl halide transferase action). The increase of negative charges goes from the blue (positive) to red (negative).

potential) are shown in red, while the most electrophilic regions (positive electrostatic potential) are shown in blue.

Considering all three carbons (C5′, C5, and CE) of SAM positioned adjacent to the sulfonium sulfur, our results show regions of positive charge predominantly on C5′, which corresponds to an electrophilic region. In this way, the attack on this carbon is facilitated so that the SalL enzyme prefers to act to form L-methionine instead of chloromethane.

Even though halide methyltransferases are promising biocatalysts for the production of halomethanes,[6,49] there is no computational study that shows in detail the reaction of this class of enzymes. However, comparing our reactant state with the structure of a SAM-dependent halide methyltransferase from *Arabidopsis thaliana* (PDB ID 3LCC)[50] we can see at least two active site residues that may be essential for methyl-halide transferase, including Val23 and Tyr172 (see Figure S2). Particularly, experimental evidence shows that the residue Tyr172 plays the role to orientate the smaller chloride nucleophile through a bridging water molecule,[50] similar to the role of Ty70 in SalL enzyme.

Interaction Energy Decomposition Analysis. The origin of the substrate−enzyme interaction can be availed by decomposing the total interaction energy on different chemical stages, such as reactant and transition states, taking into account the changes that occurred when a particular amino acid residue is removed from the enzymatic environment, as described in the method section. Then, to get suitable statistical values about this type of analysis, 400 snapshots extracted from QM/MM umbrella sampling simulations were used to compute the influence of amino acid residues 10 Å around QM region. The $\Delta\Delta E$ values for each residue indicate the degree of stabilization/destabilization of the reactant and transition states from the enzymatic environment over the QM part (Figure 6). From Figure 6, it can be observed how TS is stabilized by interactions by amino acid residues around the QM part of systems, where the positive values mean unfavorable interactions, whereas negative values correspond to favorable interactions.

To explain the differences in the $\Delta G^{\ddagger}$ between SalL−Cl, SalL−F, and SalL−HTMT systems, the interaction energy

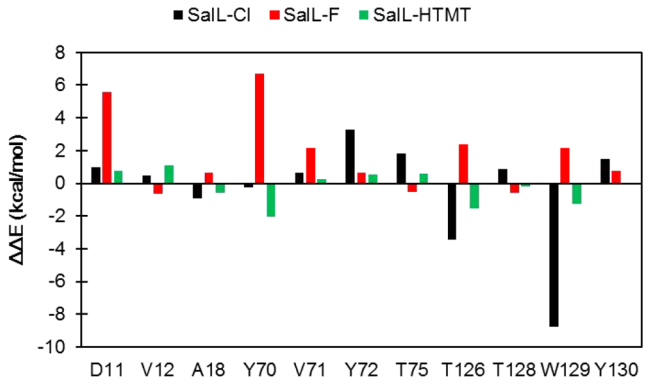

Figure 6. Relative stabilization pattern that represents the influence of amino acid residues 10 Å around the QM region on the TS considering the reactant state as reference.

decomposition approach has been used. The resultant values computed were −3.86, 19.38, and −2.43 kcal/mol, for the SalL−Cl, SalL−F, and SalL−HTMT systems, respectively. Note that the overall value of interaction energy can only explain the difference in the free energy barrier observed for SalL−Cl and SalL−F, which demonstrate that the enzyme uses key active site interactions to optimally stabilize transition state during the reaction involving the Cl^- attack. The presence of F^- ion on the SalL−F system induces a strong destabilizing effect for the majority of residues around 10 Å of QM region. Among them, we can consider the residues Trp129, Thr126, and Tyr70, which appear to be stabilizing the system with chloride and destabilizing the system with fluoride. This finding may explain the absence of enzyme activity in the presence of F^-.[7] Particularly, Tyr70 residue has a strong destabilization effect on the TS of the SalL−F system (6.70 kcal/mol), followed by the Asp60 residue (5.60 kcal/mol).

In order to explain why SalL−HTMT has a much higher barrier than SalL−Cl, we should highlight the interactions of Tyr70 and Trp129 residues: (a) Tyr70 exerts a weak stabilizing effect on the TS state of the SalL−Cl (−0.27 kcal/mol) and

https://dx.doi.org/10.1021/acs.jcim.9b01079
J. Chem. Inf. Model. 2020, 60, 738−746

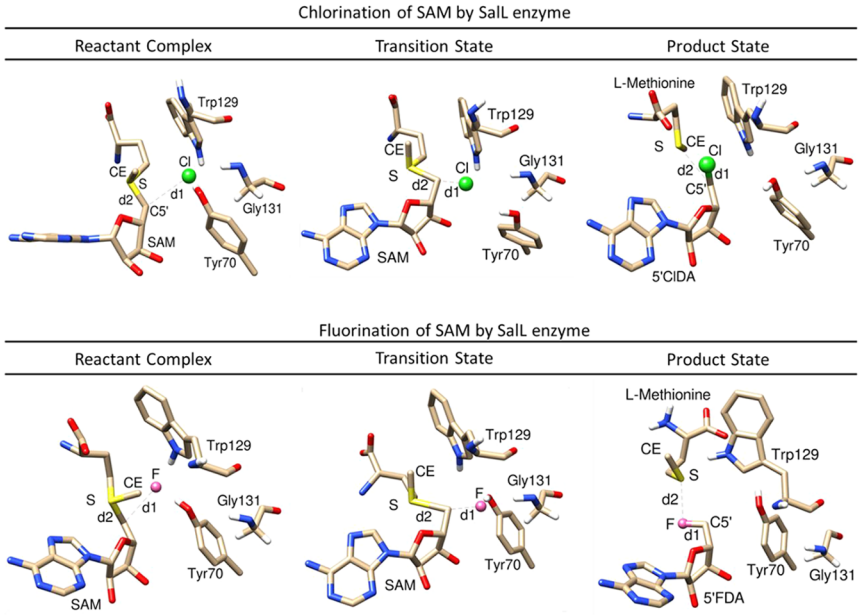

Figure 7. Representative structures of the reactant, transition, and product states for the native enzyme reaction with Cl^- and F^- halide ions. The distances values are shown in angstroms (Table 2).

SalL−HTMT (−2.06 kcal/mol) systems; (b) the Trp129 residue exerts a strong stabilizing effect on the TS state of the SalL−Cl (−8.74 kcal/mol) system and a suitable stabilizing effect on the SalL−HTMT (−1.24 kcal/mol) system. The structural influence of Trp129 occurs at the leaving group of SAM (Figure 7), where this result agrees with a more favorable halogenase activity for the SaIL enzyme.

Overall, these results suggest that the halogenase activity by Cl^- ion on the catalytic site of the SalL enzyme occurs by a strong stabilization effect on the TS. In general, SalL−Cl and SalL−HTMT systems have similar interactions for the TS state stabilization; however, Trp129 stabilizes the TS state of SalL−Cl more than SalL−HTMT, once the leaving group of halogenase reaction (L-methionine, Figure 7) is more stabilized than the SAH product from a methyl-halide transferase reaction. To the best of our knowledge, this feature has not been observed previously.

CONCLUSIONS

In this study, DFTB3/MM and free energy simulations were employed to explore the catalytic mechanism used by the SalL enzyme. Our results are in excellent agreement with kinetic data reported in the literature for the native enzyme catalyzing Cl^-. Also, we have shown that the nucleophilic reaction path is energetically preferred using chloride instead of fluoride ion ($\Delta\Delta G^{\ddagger}$ = 13.5 and 14.8 kcal/mol at the DFTB3 and M06-2X level, respectively). In other words, it has a preference to produce 5′-chloro-5′-deoxyadenosine and not 5′-fluor-5′-deoxyadenosine or chloromethane. Additionally, we have shown evidence for the fact that the residue Trp129 has an important role in stabilizing the transition state as well as Thr126. Besides that, our results showed that the residue Tyr70 plays an important role in orientating the smaller chloride nucleophile to attack C5′ and not CE in the reaction mechanism of the SalL enzyme. This occurs by a dissociative A_ND_N reaction in which there is more bond-breaking than bond-making in the transition state. Analysis of molecular electrostatic potential shows the main reasons that prevent the enzyme from acting in the formation of chloromethane. The computational studies presented here highlight the potential of QM/MM simulations as a tool for understanding the power of halogenases. Considering the fact that halogenated organic compounds have been attractive for pharmaceuticals and agrochemicals by different benefits, understanding mechanisms of SalL halogenation should be a valuable starting point in the designing of novel enzymes that may act as biocatalysts.

ASSOCIATED CONTENT

Supporting Information

The Supporting Information is available free of charge at https://pubs.acs.org/doi/10.1021/acs.jcim.9b01079.

Figure S1. Molecular electrostatic potential surface images. Figure S2. Images of the reactant state of the SalL enzyme and the active site of the HTMT enzyme. Table S1. Activation free energies (PDF)

AUTHOR INFORMATION

Corresponding Author

Anderson H. Lima − *Laboratório de Planejamento e Desenvolvimento de Fármacos, Instituto de Ciências Exatas e Naturais, Universidade Federal do Pará, Belém 66075-110, Brasil*; orcid.org/0000-0002-8451-9912; Email: anderson@ufpa.br

Authors

Paulo R. M. Pereira − *Laboratório de Planejamento e Desenvolvimento de Fármacos, Instituto de Ciências Exatas e Naturais, Universidade Federal do Pará, Belém 66075-110, Brasil*

Jéssica de O. Araújo − *Laboratório de Planejamento e Desenvolvimento de Fármacos, Instituto de Ciências Exatas e Naturais, Universidade Federal do Pará, Belém 66075-110, Brasil*

José Rogério A. Silva − *Laboratório de Planejamento e Desenvolvimento de Fármacos, Instituto de Ciências Exatas e*

https://dx.doi.org/10.1021/acs.jcim.9b01079
J. Chem. Inf. Model. 2020, 60, 738−746

Naturais, Universidade Federal do Pará, Belém 66075-110, Brasil; orcid.org/0000-0003-2310-5107

Cláudio N. Alves − *Laboratório de Planejamento e Desenvolvimento de Fármacos, Instituto de Ciências Exatas e Naturais, Universidade Federal do Pará, Belém 66075-110, Brasil;* orcid.org/0000-0001-6576-4229

Jerônimo Lameira − *Laboratório de Planejamento e Desenvolvimento de Fármacos, Instituto de Ciências Exatas e Naturais and Instituto de Ciências Biológicas, Universidade Federal do Pará, Belém 66075-110, Brasil;* orcid.org/0000-0001-7270-1517

Complete contact information is available at: https://pubs.acs.org/10.1021/acs.jcim.9b01079

Notes

The authors declare no competing financial interest.

■ ACKNOWLEDGMENTS

The authors acknowledge the National Laboratory for Scientific Computing (LNCC/MCTI, Brazil) for providing HPC resources of the SDumont supercomputer, which have contributed to the research results reported within this paper. Also, we would like to thank Conselho Nacional de Desenvolvimento Científico e Tecnológico (CNPq) for financial support. J.R.A.S. thanks the National Council for Scientific and Technological Development (CNPQ grant 407096/2016-7) for their financial support and South African Centre for High-Performance Computing (https://www.chpc.ac.za/) and University of Florida Research Computing (http://researchcomputing.ufl.edu) for providing computational resources.

■ REFERENCES

(1) Copeland, R. A.; Solomon, M. E.; Richon, V. M. Protein Methyltransferases as a Target Class for Drug Discovery. *Nat. Rev. Drug Discovery* **2009**, *8* (9), 724−732.

(2) Ayala, M.; Segovia, L.; Torres, E. Halogenases: A Biotechnological Alternative for the Synthesis of Halogenated Pharmaceuticals. *Mini-Rev. Med. Chem.* **2016**, *16* (14), 1100−1111.

(3) O'Hagan, D.; Schmidberger, J. W. Enzymes That Catalyse SN2 Reaction Mechanisms. *Nat. Prod. Rep.* **2010**, *27* (6), 900−918.

(4) Gkotsi, D. S.; Dhaliwal, J.; McLachlan, M. M.; Mulholand, K. R.; Goss, R. J. Halogenases: Powerful Tools for Biocatalysis (Mechanisms Applications and Scope). *Curr. Opin. Chem. Biol.* **2018**, *43*, 119−126.

(5) Latham, J.; Brandenburger, E.; Shepherd, S. A.; Menon, B. R. K.; Micklefield, J. Development of Halogenase Enzymes for Use in Synthesis. *Chem. Rev.* **2018**, *118* (1), 232−269.

(6) Agarwal, V.; Miles, Z. D.; Winter, J. M.; Eustáquio, A. S.; El Gamal, A. A.; Moore, B. S. Enzymatic Halogenation and Dehalogenation Reactions: Pervasive and Mechanistically Diverse. *Chem. Rev.* **2017**, *117* (8), 5619−5674.

(7) Eustáquio, A. S.; Pojer, F.; Noel, J. P.; Moore, B. S. Discovery and Characterization of a Marine Bacterial SAM-Dependent Chlorinase. *Nat. Chem. Biol.* **2008**, *4* (1), 69.

(8) Schmidberger, J. W.; James, A. B.; Edwards, R.; Naismith, J. H.; O'Hagan, D. Halomethane Biosynthesis: Structure of a SAM-Dependent Halide Methyltransferase from Arabidopsis Thaliana. *Angew. Chem., Int. Ed.* **2010**, *49* (21), 3646−3648.

(9) Dong, C.; Huang, F.; Deng, H.; Schaffrath, C.; Spencer, J. B.; O'Hagan, D.; Naismith, J. H. Crystal Structure and Mechanism of a Bacterial Fluorinating Enzyme. *Nature* **2004**, *427*, 561.

(10) Fenical, W.; Jensen, P. R.; Palladino, M. A.; Lam, K. S.; Lloyd, G. K.; Potts, B. C. Discovery and Development of the Anticancer Agent Salinosporamide A (NPI-0052). *Bioorg. Med. Chem.* **2009**, *17* (6), 2175−2180.

(11) Araújo, E.; Lima, A. H.; Lameira, J. Catalysis by Solvation Rather than the Desolvation Effect: Exploring the Catalytic Efficiency of SAM-Dependent Chlorinase. *Phys. Chem. Chem. Phys.* **2017**, *19* (32), 21350−21356.

(12) Lima, A. H.; Alves, C. N.; Prasad, R.; Lameira, J. Exploring the Origin of the Catalytic Power and Product Specificity of SET Domain Protein Methyltransferase. *Mol. BioSyst.* **2016**, *12* (10), 2980−2983.

(13) Lameira, J.; Bora, R. P.; Chu, Z. T.; Warshel, A. Methyltransferases Do Not Work by Compression, Cratic, or Desolvation Effects, but by Electrostatic Preorganization. *Proteins: Struct., Funct., Genet.* **2015**, *83* (2), 318−330.

(14) Bernstein, F. C.; Koetzle, T. F.; Williams, G. J. B.; Meyer, E. F.; Brice, M. D.; Rodgers, J. R.; Kennard, O.; Shimanouchi, T.; Tasumi, M. The Protein Data Bank. *Eur. J. Biochem.* **1977**, *80* (2), 319−324.

(15) Anandakrishnan, R.; Aguilar, B.; Onufriev, A. V. H++ 3.0: Automating PK Prediction and the Preparation of Biomolecular Structures for Atomistic Molecular Modeling and Simulations. *Nucleic Acids Res.* **2012**, *40* (W1), W537−W541.

(16) Maier, J. A.; Martinez, C.; Kasavajhala, K.; Wickstrom, L.; Hauser, K. E.; Simmerling, C. Ff14SB: Improving the Accuracy of Protein Side Chain and Backbone Parameters from Ff99SB. *J. Chem. Theory Comput.* **2015**, *11* (8), 3696−3713.

(17) Wang, J.; Wolf, R. M.; Caldwell, J. W.; Kollman, P. A.; Case, D. A. Development and Testing of a General Amber Force Field. *J. Comput. Chem.* **2004**, *25* (9), 1157−1174.

(18) Frisch, M. J. et al. *Gaussian 09*; Gaussian Inc.: Wallingford CT, 2009.

(19) Bayly, C. I.; Cieplak, P.; Cornell, W.; Kollman, P. A. A Well-Behaved Electrostatic Potential Based Method Using Charge Restraints for Deriving Atomic Charges: The RESP Model. *J. Phys. Chem.* **1993**, *97* (40), 10269−10280.

(20) Jorgensen, W. L.; Maxwell, D. S.; Tirado-Rives, J. Development and Testing of the OPLS All-Atom Force Field on Conformational Energetics and Properties of Organic Liquids. *J. Am. Chem. Soc.* **1996**, *118* (45), 11225−11236.

(21) Gaus, M.; Cui, Q.; Elstner, M. DFTB3: Extension of the Self-Consistent-Charge Density-Functional Tight-Binding Method (SCC-DFTB). *J. Chem. Theory Comput.* **2011**, *7* (4), 931−948.

(22) Hestenes, M. R.; Stiefel, E. Methods of Conjugate Gradients for Solving Linear Systems. *J. Res. Natl. Bur. Stand. (1934).* **1952**, *49* (6), 409.

(23) Roux, B. The Calculation of the Potential of Mean Force Using Computer Simulations. *Comput. Phys. Commun.* **1995**, *91* (1−3), 275−282.

(24) Riccardi, D.; Schaefer, P.; Cui, Q. PKa Calculations in Solution and Proteins with QM/MM Free Energy Perturbation Simulations: A Quantitative Test of QM/MM Protocols. *J. Phys. Chem. B* **2005**, *109* (37), 17715−17733.

(25) Silva, J. R. A.; Govender, T.; Maguire, G. E. M.; Kruger, H. G.; Lameira, J.; Roitberg, A. E.; Alves, C. N. Simulating the Inhibition Reaction of Mycobacterium Tuberculosis L, D-Transpeptidase 2 by Carbapenems. *Chem. Commun.* **2015**, *51* (63), 12560−12562.

(26) Silva, J. R. A.; Roitberg, A. E.; Alves, C. N. A QM/MM Free Energy Study of the Oxidation Mechanism of Dihydroorotate Dehydrogenase (Class 1A) from Lactococcus Lactis. *J. Phys. Chem. B* **2015**, *119* (4), 1468−1473.

(27) Alves, C. N.; Silva, J. R. A.; Roitberg, A. E. Insights into the Mechanism of Oxidation of Dihydroorotate to Orotate Catalysed by Human Class 2 Dihydroorotate Dehydrogenase: A QM/MM Free Energy Study. *Phys. Chem. Chem. Phys.* **2015**, *17* (27), 17790−17796.

(28) Pierdominici-Sottile, G.; Roitberg, A. E. Proton Transfer Facilitated by Ligand Binding. An Energetic Analysis of the Catalytic Mechanism of Trypanosoma Cruzi Trans-Sialidase. *Biochemistry* **2011**, *50* (5), 836−842.

(29) Silva, J. R. A.; Roitberg, A. E.; Alves, C. N. Catalytic Mechanism of L, D-Transpeptidase 2 from Mycobacterium Tuberculosis Described by a Computational Approach: Insights for the Design of New Antibiotics Drugs. *J. Chem. Inf. Model.* **2014**, *54* (9), 2402−2410.

(30) Wong, K.-Y.; Gao, J. The Reaction Mechanism of Paraoxon Hydrolysis by Phosphotriesterase from Combined QM/MM Simulations. *Biochemistry* **2007**, *46* (46), 13352−13369.
(31) Major, D. T.; Gao, J. A Combined Quantum Mechanical and Molecular Mechanical Study of the Reaction Mechanism and α-Amino Acidity in Alanine Racemase. *J. Am. Chem. Soc.* **2006**, *128* (50), 16345−16357.
(32) Blasiak, L. C.; Drennan, C. L. Structural Perspective on Enzymatic Halogenation. *Acc. Chem. Res.* **2009**, *42* (1), 147−155.
(33) Lienhard, G. E. Enzymatic Catalysis and Transition-State Theory. *Science (Washington, DC, U. S.)* **1973**, *180* (4082), 149−154.
(34) Eustáquio, A. S.; Härle, J.; Noel, J. P.; Moore, B. S. S-Adenosyl-L-Methionine Hydrolase (Adenosine-Forming), a Conserved Bacterial and Archeal Protein Related to SAM-Dependent Halogenases. *ChemBioChem* **2008**, *9* (14), 2215−2219.
(35) Deng, H.; Botting, C. H.; Hamilton, J. T. G.; Russell, R. J. M.; O'Hagan, D. S-Adenosyl-L-Methionine:Hydroxide Adenosyltransferase: A SAM Enzyme. *Angew. Chem., Int. Ed.* **2008**, *47* (29), 5357−5361.
(36) Deng, H.; O'Hagan, D. The Fluorinase, the Chlorinase and the Duf-62 Enzymes. *Curr. Opin. Chem. Biol.* **2008**, *12* (5), 582−592.
(37) Senn, H. M.; O'Hagan, D.; Thiel, W. Insight into Enzymatic C-F Bond Formation from QM and QM/MM Calculations. *J. Am. Chem. Soc.* **2005**, *127* (39), 13643−13655.
(38) Senn, H. M. Insights into Enzymatic Halogenation from Computational Studies. *Front. Chem.* **2014**, *2* (November), 1−15.
(39) Senn, H. M.; Kästner, J.; Breidung, J.; Thiel, W. Finite-Temperature Effects in Enzymatic Reactions — Insights from QM/MM Free-Energy Simulations. *Can. J. Chem.* **2009**, *87* (10), 1322−1337.
(40) Healy, E. F. The Effect of Desolvation on Nucleophilic Halogenase Activity. *Comput. Theor. Chem.* **2011**, *964* (1), 91−93.
(41) Jencks, W. P. A Primer for the Bema Hapothle. An Empirical Approach to the Characterization of Changing Transition-State Structures. *Chem. Rev.* **1985**, *85* (6), 511−527.
(42) Banait, N. S.; Jencks, W. P. Reactions of Anionic Nucleophiles with. Alpha.-D-Glucopyranosyl Fluoride in Aqueous Solution through a Concerted, ANDN (SN2) Mechanism. *J. Am. Chem. Soc.* **1991**, *113* (21), 7951−7958.
(43) Pierdominici-Sottile, G.; Horenstein, N. A.; Roitberg, A. E. Free Energy Study of the Catalytic Mechanism of Trypanosoma Cruzi Trans-Sialidase. From the Michaelis Complex to the Covalent Intermediate. *Biochemistry* **2011**, *50* (46), 10150−10158.
(44) Pauling, L. Atomic Radii and Interatomic Distances in Metals. *J. Am. Chem. Soc.* **1947**, *69* (3), 542−553.
(45) Houk, K. N.; Gustafson, S. M.; Black, K. A. Theoretical Secondary Kinetic Isotope Effects and the Interpretation of Transition State Geometries. 1. The Cope Rearrangement. *J. Am. Chem. Soc.* **1992**, *114* (22), 8565−8572.
(46) Deng, H.; McMahon, S. A.; Eustáquio, A. S.; Moore, B. S.; Naismith, J. H.; O'Hagan, D. Mechanistic Insights into Water Activation in SAM Hydroxide Adenosyltransferase (Duf-62). *ChemBioChem* **2009**, *10* (15), 2455−2459.
(47) Lameira, J.; Alves, C. N.; Tuñón, I.; Martí, S.; Moliner, V. Enzyme Molecular Mechanism as a Starting Point to Design New Inhibitors: A Theoretical Study of O-GlcNAcase. *J. Phys. Chem. B* **2011**, *115* (20), 6764−6775.
(48) Carneiro, A. S.; Lameira, J.; Alves, C. N. A Theoretical Study of the Molecular Mechanism of the GAPDH Trypanosoma Cruzi Enzyme Involving Iodoacetate Inhibitor. *Chem. Phys. Lett.* **2011**, *514* (4−6), 336−340.
(49) Bayer, T. S.; Widmaier, D. M.; Temme, K.; Mirsky, E. A.; Santi, D. V.; Voigt, C. A. Synthesis of Methyl Halides from Biomass Using Engineered Microbes. *J. Am. Chem. Soc.* **2009**, *131* (18), 6508−6515.
(50) Schmidberger, J. W.; James, A. B.; Edwards, R.; Naismith, J. H.; O'Hagan, D. Halomethane Biosynthesis: Structure of a SAM-Dependent Halide Methyltransferase from Arabidopsis Thaliana. *Angew. Chem., Int. Ed.* **2010**, *49* (21), 3646−3648.

https://dx.doi.org/10.1021/acs.jcim.9b01079
J. Chem. Inf. Model. 2020, 60, 738−746